Selective $Na_V1.1$ activation rescues Dravet syndrome mice from seizures and premature death

Kay L. Richards[a,1], Carol J. Milligan[a,1], Robert J. Richardson[a], Nikola Jancovski[a], Morten Grunnet[b,c], Laura H. Jacobson[d,e], Eivind A. B. Undheim[f], Mehdi Mobli[f], Chun Yuen Chow[g], Volker Herzig[g], Agota Csoti[h], Gyorgy Panyi[h], Christopher A. Reid[a,i], Glenn F. King[g,2,3], and Steven Petrou[a,i,2,3]

[a]Ion Channels and Disease Group, Florey Institute of Neuroscience and Mental Health, Parkville, VIC 3010, Australia; [b]Neuroscience Drug Discovery, H. Lundbeck A/S, DK-2500 Valby, Denmark; [c]Department of Drug Design and Pharmacology, Copenhagen University, DK-2100 Copenhagen, Denmark; [d]Sleep and Cognition Group, Epilepsy Division, Florey Insitute of Neuroscience and Mental Health, Parkville, VIC 3010, Australia; [e]Department of Pharmacology and Therapeutics, The University of Melbourne, Parkville, VIC 3010, Australia; [f]Centre for Advanced Imaging, The University of Queensland, Brisbane, QLD 4072, Australia; [g]Institute for Molecular Bioscience, The University of Queensland, Brisbane, QLD 4072, Australia; [h]Department of Biophysics and Cell Biology, Faculty of Medicine, University of Debrecen, H-4032 Debrecen, Hungary; and [i]Department of Medicine, The University of Melbourne, Parkville, VIC 3010, Australia

Edited by Francisco Bezanilla, The University of Chicago, Chicago, IL, and approved June 29, 2018 (received for review March 22, 2018)

Dravet syndrome is a catastrophic, pharmacoresistant epileptic encephalopathy. Disease onset occurs in the first year of life, followed by developmental delay with cognitive and behavioral dysfunction and substantially elevated risk of premature death. The majority of affected individuals harbor a loss-of-function mutation in one allele of *SCN1A*, which encodes the voltage-gated sodium channel $Na_V1.1$. Brain $Na_V1.1$ is primarily localized to fast-spiking inhibitory interneurons; thus the mechanism of epileptogenesis in Dravet syndrome is hypothesized to be reduced inhibitory neurotransmission leading to brain hyperexcitability. We show that selective activation of $Na_V1.1$ by venom peptide Hm1a restores the function of inhibitory interneurons from Dravet syndrome mice without affecting the firing of excitatory neurons. Intracerebroventricular infusion of Hm1a rescues Dravet syndrome mice from seizures and premature death. This precision medicine approach, which specifically targets the molecular deficit in Dravet syndrome, presents an opportunity for treatment of this intractable epilepsy.

genetic epilepsy | targeted drug therapy | seizures | Dravet syndrome | spider venom

Dravet syndrome is a catastrophic pediatric epilepsy characterized by childhood onset of intractable polymorphic seizures accompanied by cognitive impairment, psychomotor regression, autistic traits, and ataxia (1–4). Clinically it presents as one of the most pharmacoresistant epilepsy syndromes (5). Further, the incidence of sudden unexpected death in epilepsy is 30-fold higher in Dravet syndrome than in other childhood-onset epilepsies, accounting for up to 50–60% of mortality (4, 6). Therefore there is an urgent need to develop new therapeutic strategies to treat this devastating disease.

About 80% of Dravet syndrome cases result from de novo heterozygous loss-of-function mutations in *SCN1A*, which encodes the voltage-gated sodium channel $Na_V1.1$ (7, 8). In the brain, $Na_V1.1$ is expressed predominantly in the axon initial segment of fast-spiking parvalbumin-positive (Pv^+) GABAergic inhibitory interneurons (9). Selective reduction of $Na_V1.1$ expression in Pv^+ interneurons is sufficient to recapitulate many of the clinical symptoms of Dravet syndrome (9–13). A potential clinical correlate of this mechanism is that sodium-channel blockers, which will normally work in an antiepileptic fashion, can make symptoms worse in some Dravet syndrome patients (10, 14). This might be explained by decreased inhibitory neuron firing, which in these patients has a devastating impact that cannot be compensated by sodium-channel inhibition on excitable neurons (10, 14). In contrast, for Dravet syndrome patients, compounds that enhance GABAergic neurotransmission are more effective anticonvulsants (8, 15).

Precision therapies that rescue $Na_V1.1$ haploinsufficiency should therefore be clinically effective and reduce seizures and attendant comorbidities. Hm1a is a spider venom peptide that selectively potentiates $Na_V1.1$ channels (16). It does so by inhibiting gating movement of the domain IV (DIV) voltage sensor of $Na_V1.1$, which hinders both fast and slow inactivation of the channel and leads to a persistent current at depolarized potentials (16, 17). Hm1a is therefore an obvious candidate for a precision therapy that targets WT channels in patients with Dravet syndrome.

The ability of Hm1a to rescue $Na_V1.1$ haploinsufficiency was evaluated in a mouse model of Dravet syndrome in which the mouse carries one mutated and one unaffected allele (9). Hm1a selectivity was confirmed in a heterologous expression system with preferential action on $hNa_V1.1$ channels over other Na_V

Significance

Spider venom is a rich source of peptides, many targeting ion channels. We assessed a venom peptide, Hm1a, as a potential targeted therapy for Dravet syndrome, the genetic epilepsy linked to a mutation in the gene encoding the sodium channel alpha subunit $Na_V1.1$. Cell-based assays showed Hm1a was selective for $hNa_V1.1$ over other sodium and potassium channels. Utilizing a mouse model of Dravet syndrome, Hm1a restored inhibitory neuron function and significantly reduced seizures and mortality in heterozygote mice. Evidence from the structure of Hm1a and modeling suggest Hm1a interacts with $Na_V1.1$ inactivation domains, providing a structural correlate of the functional mechanisms. This proof-of-concept study provides a promising strategy for future drug development in genetic epilepsy and other neurogenetic disorders.

Author contributions: K.L.R., C.J.M., E.A.B.U., M.M., C.Y.C., V.H., G.P., C.A.R., G.F.K., and S.P. designed research; K.L.R., C.J.M., R.J.R., N.J., M.G., E.A.B.U., M.M., C.Y.C., V.H., and A.C. performed research; L.H.J. contributed new reagents/analytic tools; K.L.R., C.J.M., N.J., M.G., E.A.B.U., M.M., C.Y.C., V.H., A.C., G.P., C.A.R., G.F.K., and S.P. analyzed data; and K.L.R., C.J.M., R.J.R., N.J., M.G., L.H.J., E.A.B.U., M.M., C.Y.C., V.H., A.C., G.P., C.A.R., G.F.K., and S.P. wrote the paper.

Conflict of interest: G.F.K. and S.P. are listed as inventors on a patent application on Hm1a (WO/2017/096431).

This article is a PNAS Direct Submission.

Data deposition: The chemical shifts reported in this paper have been deposited in the Biological Magnetic Resonance Data Bank (accession no. 25775), and the atomic coordinates for the structures reported in this paper have been deposited in the Protein Data Bank, www.wwpdb.org (PDB ID code 2N6O).

[1]K.L.R. and C.J.M. contributed equally to this work.

[2]G.F.K. and S.P. contributed equally to this work.

[3]To whom correspondence may be addressed. Email: glenn.king@imb.uq.edu.au or spetrou@unimelb.edu.au.

This article contains supporting information online at www.pnas.org/lookup/suppl/doi:10.1073/pnas.1804764115/-/DCSupplemental.

Published online August 3, 2018.

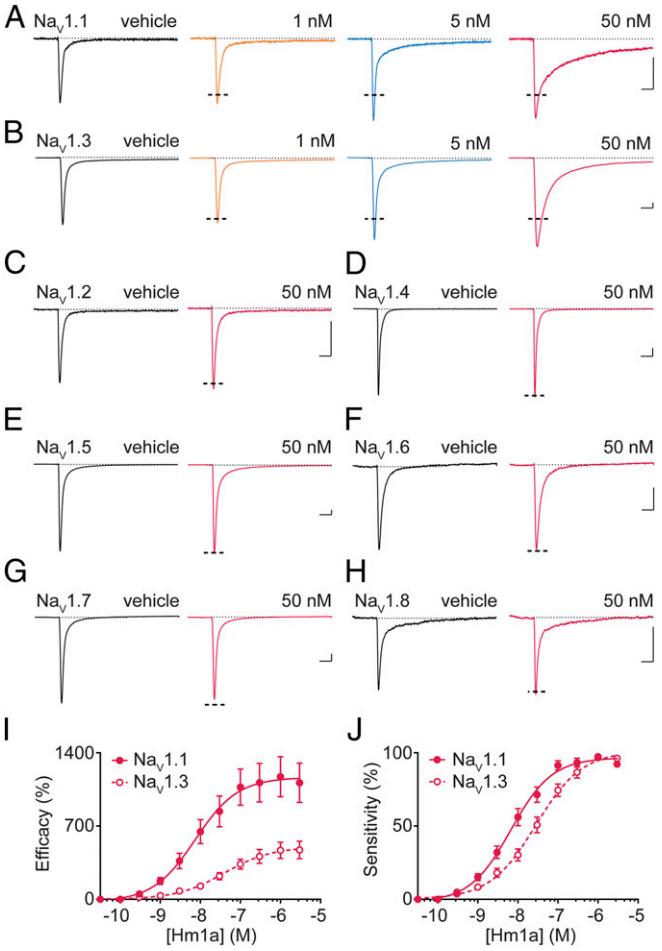

Fig. 1. The effect of Hm1a on voltage-gated sodium channel subtypes hNa$_V$1.1–hNa$_V$1.8 stably expressed in HEK293T or CHO cells. (*A*) Representative raw current traces for hNa$_V$1.1 in the presence of vehicle (black trace) or 1 nM (orange trace), 5 nM (blue trace), or 50 nM (pink trace) Hm1a. (*B*) Representative raw current traces for hNa$_V$1.3 in the presence of vehicle (black trace) or 1 nM (orange trace), 5 nM (blue trace), or 50 nM (pink trace) Hm1a. (*C–H*) Representative raw current traces for hNa$_V$1.2, hNa$_V$1.4, hNa$_V$1.5, hNa$_V$1.6, hNa$_V$1.7, and hNa$_V$1.8 in the presence of vehicle (black traces) or 50 nM (pink traces) Hm1a, respectively. All traces are averaged over 30-s periods. (Scale bars: 2 ms horizontal; 200 pA vertical.) (*I*) Efficacy as a function of Hm1a concentration for Na$_V$1.1 (●) and Na$_V$1.3 (○). Data points are the mean ± SEM of nine independent cells for hNa$_V$1.1 and of 10 independent cells for hNa$_V$1.3. Curve fitting yielded EC$_{50}$ values of 7.5 ± 0.2 nM and 39.5 ± 0.2 nM for hNa$_V$1.1 and hNa$_V$1.3, respectively. (*J*) Sensitivity as a function of Hm1a concentration for Na$_V$1.1 (●) and Na$_V$1.3 (○). Curve fitting yielded EC$_{50}$ values of 6.7 ± 0.1 nM and 28.1 ± 0.1 nM for hNa$_V$1.1 and hNa$_V$1.3, respectively.

channels and was without significant action on voltage-gated potassium (K$_V$) channels. Hm1a rescued action potential (AP) firing in GABAergic interneurons from Dravet syndrome mice and spared excitatory neuron firing. Hm1a treatment in Dravet syndrome mice showed remarkable efficacy with a significant reduction in seizure counts and mortality. This study demonstrates that a precision-medicine strategy that targets fundamental disease mechanisms can achieve efficacy in an otherwise refractory disease.

Results

Hm1a Delays Na$_V$1.1 Inactivation. Hm1a was previously shown to be highly selective for Na$_V$1.1 over Na$_V$1.2–Na$_V$1.8 when the α subunits alone were expressed in *Xenopus* oocytes (16). However, since the pharmacology of venom-derived sodium-channel toxins can be influenced by auxiliary subunits (18) and post-translational channel modifications (19), we employed automated planar patch-clamp electrophysiology to reexamine Hm1a selectivity using mammalian cells expressing human (h) Na$_V$1.1–Na$_V$1.8 in the presence of the human sodium channel β1 subunit. At concentrations ≥5 nM Hm1a enhanced hNa$_V$1.1 peak current amplitude and potently delayed channel inactivation in a dose-dependent manner, leading to a large sustained current (Fig. 1*A*). A similar action was seen on hNa$_V$1.3 channels (Fig. 1*B*), although with lower efficacy (a measurement of the magnitude of change in total charge versus peptide concentration) and lower sensitivity (calculated as a change in response versus concentration, compared with hNa$_V$1.1) (Fig. 1 *I* and *J*). Application of up to 50 nM Hm1a had no effect on other hNa$_V$ subtypes (Fig. 1 *C–H* and *SI Appendix*, Fig. S1).

We next examined the effect of Hm1a on biophysical properties of hNa$_V$1.1. Current family traces illustrate potent inhibition of hNa$_V$1.1 inactivation by 5 nM Hm1a (Fig. 2*A*). Hm1a had no effect on the voltage dependence of steady-state activation (Fig. 2*B*) and at 50 nM induced a significant depolarizing shift in the voltage dependence of inactivation (Fig. 2*B*). With increasing concentration of Hm1a, the slope factor of the steady-state inactivation curve increased (Fig. 2*B*). The effect of Hm1a on Na$_V$1.1 inactivation was quantified by fitting a double exponential curve. The time constant of fast inactivation was significantly increased at 50 nM (Fig. 2*C*). A significant slowing of inactivation was also seen at the lower concentration of 5 nM (Fig. 2*D*), resulting in the appearance of a persistent current across the entire duration of the voltage step (Fig. 2*E*). Hm1a did not have any impact on recovery from fast inactivation (Fig. 2*F*).

Hm1a Does Not Modulate K$_V$ Channels. Hm1a was previously shown to have no effect on K$_V$1.1–K$_V$1.6 and K$_V$3.4, but it was reported to be a weak inhibitor of K$_V$2.2, K$_V$4.1, and K$_V$4.3 (IC$_{50}$ ~ 300 nM) (20). The lack of data on calcium-activated potassium (K$_{Ca}$) channels and biologically important K$_V$ channels such as K$_V$11.1 (hERG) motivated the extension of the selectivity profile of Hm1a (20). At a concentration of 300 nM (i.e., 25-fold higher than the EC$_{50}$ on Na$_V$1.1), Hm1a had no significant effect on K$_V$1.7, K$_V$10.1 (hEAG), K$_V$11.1 (hERG), K$_{Ca}$1.1, K$_{Ca}$2.2, or K$_{Ca}$3.1 (*SI Appendix*, Figs. S2 and S3).

Hm1a Is a Knottin Peptide with Moderate in Vivo Stability. We produced recombinant Hm1a and determined its structure using 2D homonuclear NMR techniques. The final ensemble of NMR-derived structures is high resolution based on measures of precision (backbone rmsd of 0.18 ± 0.04 Å) and stereochemical quality (*SI Appendix*, Table S1) (21). The structure of Hm1a (Fig. 3*A* and *SI Appendix*, Fig. S4) reveals a classical knottin fold in which a central β-hairpin is stabilized by three disulfide bonds that form an inhibitor cystine knot (ICK) motif (Fig. 3*B*) (22). The Cys2–Cys16 and Cys9–Cys21 disulfide bonds and the intervening sections of the polypeptide backbone form a 14-residue ring that is pierced by the Cys15–Cys28 disulfide bond to form the cystine knot (Fig. 3*C*).

One face of the Hm1a structure is comprised of a set of contiguous hydrophobic residues (Tyr4, Leu5, Phe6, Tyr27, Trp30, and Phe34) (Fig. 3*D*, *Left*) that are conserved in the paralogous toxin Hm1b, which has similar pharmacology (16). This face of the peptide likely mediates the interaction between Hm1a and Na$_V$1.1, since all the residues that differ between Hm1a and Hm1b form a spine on the opposite face of the molecule (Fig. 3*D*, *Right*). We previously showed that both the S1–S2 and S3–S4 extracellular loops of the domain IV voltage sensor of Na$_V$1.1 are important for recognition of Hm1a (16), and hence we propose that Hm1a engages the channel by lodging into the water-filled cavity between the S1–S2 and S3–S4 helical bundles and acts as a wedge that impedes outward movement of

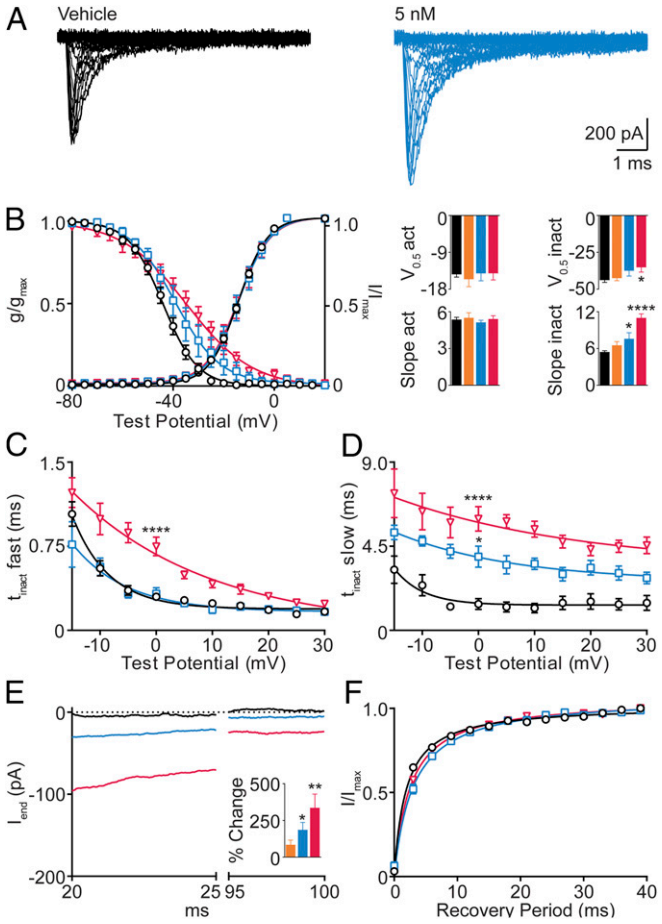

Fig. 2. Hm1a alters the biophysical properties of the hNa$_V$1.1 channel. (*A*) Representative traces for vehicle (black traces) and 5 nM Hm1a (blue traces). (*B*) Voltage dependence of normalized peak conductance (g/g_{max}) and steady-state inactivation (I/I_{max}) for vehicle (black circles) and 5 nM (blue squares) and 50 nM (pink triangles) Hm1a. (*Insets*) Biophysical parameters for vehicle (black bars) or 1 (orange bars), 5 (blue bars), or 50 nM (pink bars) Hm1a. Peptide caused a significant shift in I/I_{max}: $V_{0.5}$ inactivation (inact) = −35.3 ± 1.8 mV vehicle vs. −45.9 ± 1.3 mV Hm1a 50 nM; slope inact = 5.4 ± 0.5 vehicle vs. 7.6 ± 0.9 Hm1a 5 nM, vs. 11.0 ± 0.7 Hm1a 50 nM. (*C*) Time constant of fast inactivation (t_{inact} fast) for vehicle (black circles), 5 nM (blue squares) and 50 nM (pink triangles) Hm1a as a function of voltage. At peak current (0 mV) Hm1a (50 nM) causes a significant increase in t_{inact} fast (t_{inact} fast = 0.31 ± 0.03 ms vehicle vs. 0.75 ± 0.3 ms Hm1a 50 nM). (*D*) Time constant of slow inactivation (t_{inact} slow) shown for vehicle (black circles), 5 nM (blue squares) and 50 nM (pink triangles) Hm1a. At peak current (0 mV), Hm1a (5 and 50 nM) causes significant increases in t_{inact} slow (t_{inact} slow = 1.4 ± 0.4 ms vehicle vs. 3.94 ± 0.6 ms Hm1a 5 nM vs. 5.97 ± 0.74 ms Hm1a 50 nM). In *C* and *D* the current for each cell was fitted to a double exponential at a range of test potentials and time constants determined. A one-phase exponential decay was fitted to pooled averages. (*E*) Sustained currents for vehicle (black trace), 5 nM (blue trace) 50 nM (pink trace) Hm1a. (*Inset*) Mean percentage change in end current for 1 nM (orange bar), 5 nM (blue bar), and 50 nM (pink bar) Hm1a ($n = 6$ cells). (*F*) Recovery of channel availability from fast-inactivation shown for vehicle (black circles), 5 nM (blue squares) and 50 nM (pink triangle) Hm1a as a function of time. A hyperbola was fitted to pooled averages. *$P < 0.05$; **$P < 0.01$; ****$P < 0.0001$. Comparisons were made between the vehicle ($n = 32$) and 1 nM ($n = 6$), 5 nM ($n = 10$), and 50 nM ($n = 12$) Hm1a.

the DIV voltage sensor during membrane depolarization. Hm1a most likely engages the channel with its hydrophobic face pointing into the DIV cavity, making contacts with both the S1–S2 and S3–S4 helices, while the poorly conserved and largely polar opposing face points toward the extracellular space (Fig. 3*E*).

Stability of the peptide was analyzed in an isolated cerebrospinal fluid (CSF) preparation (Fig. 3*F*). The knotted architecture of ICK peptides typically provides them with very high levels of stability in serum and other biological fluids (23), but their stability in CSF is mostly unknown. We found that Hm1a is more stable than human atrial natriuretic peptide (hANP) in human CSF but is significantly less stable than ziconotide, a venom-derived ICK peptide drug that is administered intrathecally for treatment of intractable chronic pain (24).

Hm1a Rescues Interneuron Function from Dravet Syndrome Mice. Mice carrying an *Scn1a* variant identified in human Dravet syndrome (R1407X), bred into a mixed C57BL/6J/129S1/SvImJ background, developed spontaneous seizures and early mortality (9, 25). Whole-cell recordings from interneurons in the CA1 stratum radiatum of these Dravet syndrome mice were made to assess the effect of Hm1a on AP firing activity. Collapse of AP firing at current injections >300 pA was a robust cellular phenotype in Dravet syndrome mice interneurons (Fig. 4 *A–D*), confirming previous findings (9, 26). Remarkably, 10 nM Hm1a rescued the AP firing deficit with average AP count significantly greater than control for current injections >300 pA (Fig. 4 *A* and *B*).

Detailed analysis of nine sequential APs at a current step that elicited collapse was also made (Fig. 4 *C–E*). Interestingly, Hm1a caused no significant change in the amplitude of the first few APs, but increased the amplitude of subsequent APs (Fig. 4 *C* and *D*). The waveform of the first AP elicited at rheobase was unchanged in the presence of the peptide (Fig. 4*E*). Hm1a induced a small increase in rheobase current (baseline, 59 ± 10 vs. Hm1a, 81 ± 13 pA, $P < 0.01$, $n = 10$; paired *t* test) as well as a depolarizing shift in threshold voltage (44 ± 2 vs. 36 ± 4 mV, $P < 0.02$, $n = 10$; paired *t* test) and resting membrane potential (77 ± 1 vs. 73 ± 1 mV, $P < 0.02$, $n = 10$; paired *t* test), but had no impact on input resistance (550 ± 73 vs. 460 ± 60 MΩ; $P = 0.11$, $n = 10$; paired *t* test).

Hm1a Does Not Alter Firing of GABAergic Interneurons from WT Mice or Excitatory Neurons from Dravet Syndrome Mice. Hm1a had minimal impact on the firing properties of noncollapsing WT CA1 GABAergic interneurons (Fig. 5 *A–C*, $n = 6$). There were no significant differences in the amplitude, rise time, width, and threshold of APs at rheobase (Fig. 5*C*). Further, Hm1a had no effect on rheobase (111 ± 18 vs. 123 ± 18 pA, $P = 0.5$, $n = 6$; paired *t* test) and caused a nonsignificant right shift in the input current vs action potential output (*i–o*) relationship at intermediate current injections (Fig. 5*B*). Hm1a also had no impact on resting membrane potential (Fig. 5*C*) or input resistance (270 ± 40 vs. 330 ± 40 MΩ, $P = 0.76$, $n = 6$; paired *t* test).

Hm1a (10 nM) had no impact on the firing properties of CA1 pyramidal neurons recorded from Dravet syndrome mice (Fig. 5 *D–F*), consistent with reports that Na$_V$1.1 expression in brain is primarily localized to GABAergic interneurons (9, 26). Hm1a caused a small depolarizing shift in resting membrane potential (Fig. 5*F*), but had no impact on input resistance (450 ± 70 vs. 420 ± 60 MΩ, $P = 0.8$, $n = 6$; paired *t* test), rheobase (98 ± 15 vs. 101 ± 16 pA, $P = 0.8$, $n = 6$; paired *t* test), or the amplitude, rise time, width, and threshold of APs measured at rheobase (Fig. 5*F*).

Acute Hm1a Infusion Reduces Whole-Brain Hyperexcitability in Dravet Syndrome Mice. To overcome poor CNS availability of systemically delivered peptides, we used intracerebroventricular (ICV) delivery for in vivo tests of Hm1a efficacy. After postnatal day (P)19, electrocorticography (ECoG) recordings from Dravet syndrome mice revealed high-amplitude interictal epileptiform discharges or "spikes" (Fig. 6*A* and *SI Appendix*, Fig. S5), which were used as a biomarker for assessing Hm1a efficacy.

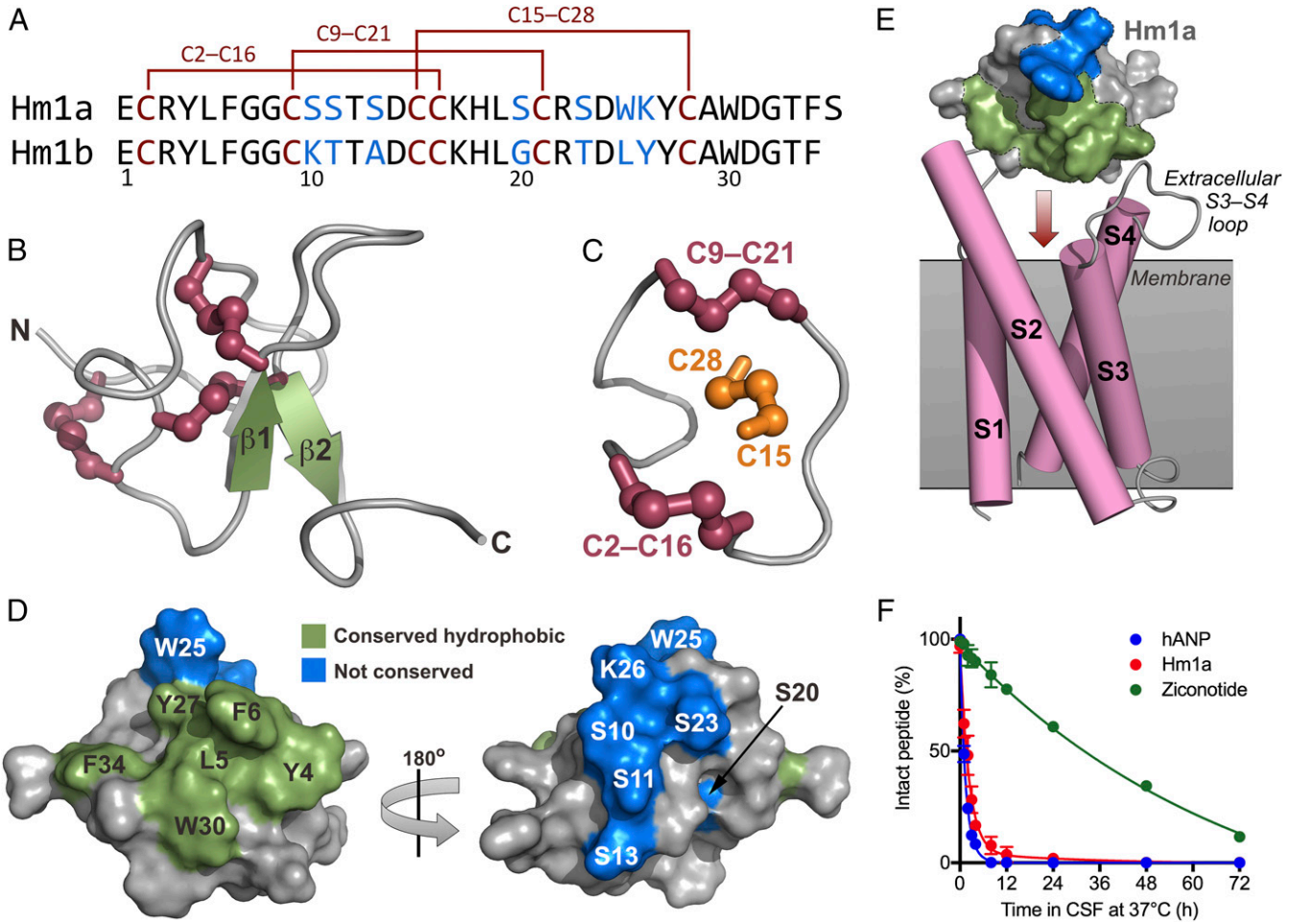

Fig. 3. Structure and stability of Hm1a. (*A*) Primary structures of Hm1a and Hm1b. Nonconserved residues are highlighted in blue. The disulfide-bond architecture is illustrated above the sequences. (*B*) 3D structure of Hm1a. Disulfide bonds are shown in red, β strands are green, and the N- and C-termini are labeled. (*C*) Cystine knot motif in Hm1a. The C15–C28 disulfide bond (orange) bisects a closed loop formed by the other two disulfide bonds (red) and the intervening sections of peptide backbone (gray). (*D*) Surface representation of Hm1a showing exposed hydrophobic residues that are conserved in Hm1b (green) and residues that differ between Hm1a and Hm1b (blue). (*E*) Speculative model for interaction of the hydrophobic face of Hm1a with the DIV voltage sensor of $Na_V1.1$. (*F*) Stability of Hm1a, hANP, and ziconotide in human CSF.

Spike analysis was conducted before, during, and after acute ICV infusion of 5 μL of 0.5 μM Hm1a, dissolved in saline and fatty-acid free BSA (fafBSA) vehicle, delivered over a period of 1 h.

In contrast to the significant spike activity observed before Hm1a infusion, very few high-amplitude spike events were detected in ECoG recordings 1 h after Hm1a administration (Fig. 6). Power spectrum analysis for a 30-min epoch showed peak activity at 0.5–2 Hz before Hm1a delivery, and this was significantly reduced by Hm1a infusion (Fig. 6*B* and *SI Appendix*, Table S2). Average spike frequency in Dravet syndrome mice was significantly reduced by Hm1a infusion (Fig. 6*C*). There was no difference in spike frequency in Dravet syndrome mice measured before and after vehicle infusion (27.5 spikes/h [95% CI 0.07–54.9] preinfusion versus 24.5 spikes/h [95% CI −0.910–49.9] postinfusion; $P = 0.19$; $n = 4$).

We observed a spike-free period of ∼1 h following the cessation of Hm1a infusion (*SI Appendix*, Fig. S6), which likely correlates with a gradual clearance and/or metabolism of peptide within the CSF. The in vitro half-life for Hm1a in CSF (∼1.7 h) (Fig. 3*F*) closely mirrored the spike-free period following cessation of Hm1a infusion.

Long-Term Hm1a Infusion Reduces Seizures and Mortality in Dravet Syndrome Mice. Previous studies have shown that survival of Dravet syndrome mice is reduced from P17 (9). Our cohort of Dravet syndrome mice out-crossed with C57BL/6J (N2, second backcross generation) also had dramatically decreased survival compared with WT littermates (Fig. 7*A*). The mortality of heterozygous Dravet syndrome mice was highest between P18 and P26. Video and visual observation showed that mortality was always correlated with a preceding spontaneous seizure event. We used this high seizure and mortality epoch to assess the impact of long-term Hm1a infusion. Video monitoring was performed from P18 for the duration of the experiment. Mice that displayed a minimum of two seizures qualified as subjects for long-term efficacy trials and were randomly assigned to either the Hm1a-treated or the vehicle-treated groups. At initiation of the trial, average seizure frequencies were identical for the treatment and control groups (Fig. 7*B*).

During continuous Hm1a infusion, seizure frequency was significantly reduced or completely abolished in six of nine mice (67%) after 3 d. In contrast, seizure frequency increased dramatically in the control group (Fig. 7*B*). In the first 24-h period after control infusion was initiated, 62% of mice had died (Fig. 7*C*), and by day 3 all control-treated mice were dead. Hm1a infusion caused no obvious adverse events; Hm1a-treated mice displayed normal home cage activity, including eating, drinking, and grooming behavior [see Movies S1 and S2 for examples of

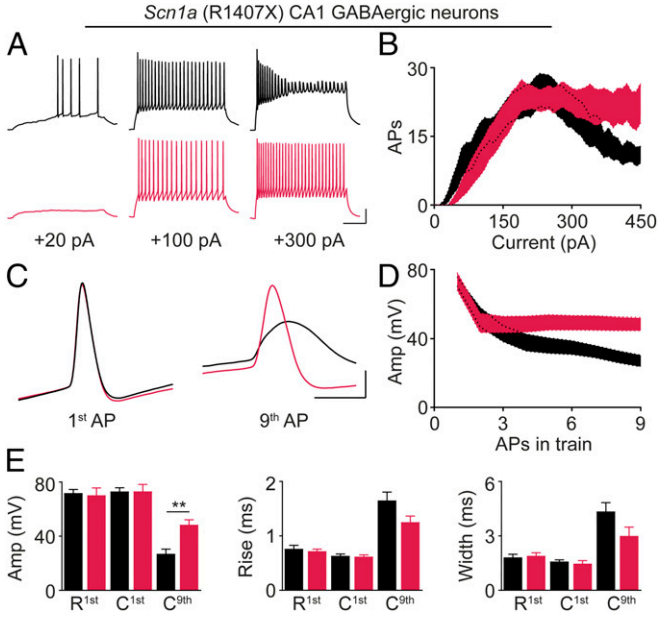

Fig. 4. Hm1a reverses AP firing collapse in Dravet syndrome mice CA1 GABAergic neurons. (*A*, *Upper*) Raw traces recorded from single CA1 GABAergic neuron at progressively more depolarizing current injections. (*A*, *Lower*) Raw traces from the same neuron following the addition of Hm1a (10 nM). (Scale bars: 200 ms horizontal; 20 mV vertical.) (*B*) Summary of *i–o* data. Control (black) and Hm1a-treated (pink) show the recovery of AP collapse in the presence of the peptide (AP counts at >300 pA; $P < 0.02$, $n = 10$, paired *t* test). (*C*) Raw traces (control, black trace; Hm1a, pink trace) of the first and ninth individual APs from a train of APs at the point of collapse. (Scale bars: 5 ms horizontal; 20 mV vertical.) (*D*) Summary of peak AP amplitude (control, black; Hm1a, pink) of sequential APs in a train. The amplitude of the fourth to ninth APs is significantly larger in Hm1a-treated cells than untreated, control cells. $P < 0.04$, paired *t* test. (*E*) Morphology of the first AP at rheobase (R^{1st}) and the first AP (C^{1st}) and ninth AP (C^{9th}) at a current injection causing collapse. Control, black bars; Hm1a, pink bars; $^{**}P < 0.005$, paired *t* test).

four Dravet syndrome mice before (Movie S1) and during (Movie S2) Hm1a infusion].

Discussion

The aim of this study was to assess the utility of the venom peptide Hm1a as a targeted treatment for Dravet syndrome caused by loss of $Na_V1.1$ function. We demonstrated that Hm1a enhances $Na_V1.1$ currents, rescues an interneuron AP firing deficit, and reduces seizure susceptibility and mortality in a mouse model of Dravet syndrome. Our results provide strong proof of concept that therapy based on directly targeting a molecular deficit in intractable epilepsy is feasible, providing a promising strategy for future drug development in genetic epilepsy and other neurogenetic disorders.

The primary effect of Hm1a on $hNa_V1.1$ was to delay fast inactivation, which led to a substantial persistent current. Hm1a had a similar impact on $hNa_V1.3$ channels, although with lower efficacy and sensitivity, and had no effect on other Na_V channels. Our results differ subtly from those previously reported, in which Hm1a had little effect on $Na_V1.3$ but altered peak current and inactivation in $Na_V1.2$ channels (16). These earlier data were obtained using *Xenopus* oocytes without coexpression of auxiliary β1 subunits, while data from this study were obtained using mammalian cells expressing this subunit.

The lack of efficacy at $Na_V1.2$ demonstrated here is an important point, as drugs that potentiate $Na_V1.2$ would likely be proepileptic and certainly would be contraindicated in Dravet syndrome. The weak activity of Hm1a at $Na_V1.3$ is likely to have minimal effect on neuronal function. In both rodent and human brain, there is a continuous postnatal increase in $Na_V1.1$ levels, whereas $Na_V1.3$ expression is highest just before birth, with a rapid postnatal decline (27, 28), with no compensatory upregulation of expression occurring in the Dravet syndrome mice (9). Essentially, the mean age at seizure onset in Dravet syndrome patients (5.7 mo) closely approximates the point at which the increasing level of $Na_V1.1$ exceeds the diminishing level of $Na_V1.3$ in normal human brain development (27).

Recently identified is the role that $Na_V1.1$ also plays in transduction of mechanical pain via primary sensory afferents in the peripheral nervous system (16, 17). $Na_V1.1$ activators therefore may enhance the sensation of pain if given systemically. It is important to note that Dravet patients are haploinsufficient for $Na_V1.1$ and therefore may be less sensitive to this effect. Furthermore, Hm1a delivered directly within the CNS is unlikely to result in elevated pain sensitivity, and this is consistent with mice showing no overt adverse effects to ICV infusion of Hm1a.

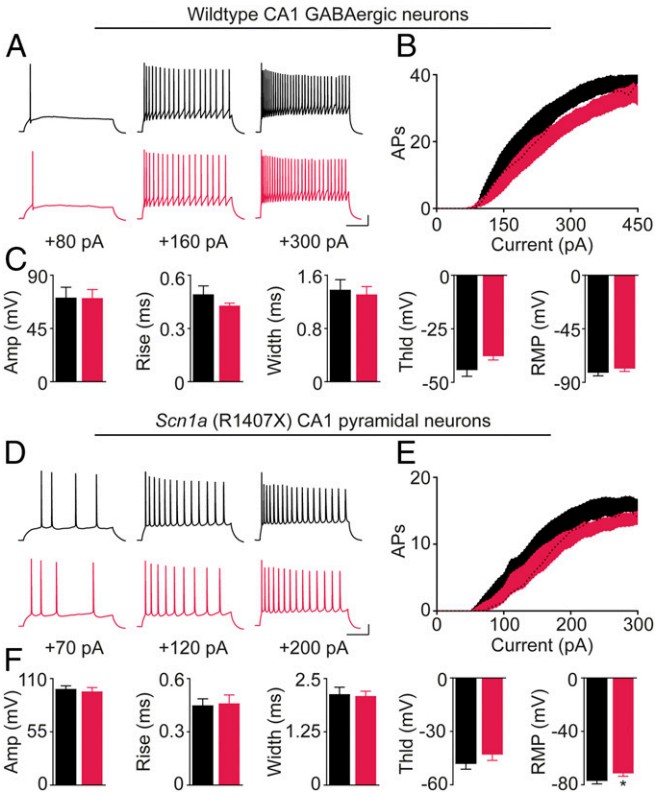

Fig. 5. Hm1a has no impact on WT GABAergic or pyramidal CA1 neurons of Dravet mice. (*A*, *Upper*) Raw traces (black) recorded from single WT CA1 GABAergic neuron at progressively more depolarizing current injections. (*Lower*) Raw traces (pink) from the same neuron following the addition of Hm1a (10 nM). (Scale bars: 200 ms; 20 mV vertical.) (*B*) Summary of *i–o* data. Control (black) and Hm1a (pink) data ($n = 6$) indicate a small right shift in the relationship at intermediate current injections that normalized at higher currents in the presence of the Hm1a. (*C*) No significant change in AP amplitude, rise, width, or threshold was detected at rheobase or resting membrane potential in WT GABAergic neurons shown without (black bars) and with (pink bars) Hm1a. (*D*, *Upper*) Raw traces (black) recorded from a single mutant CA1 pyramidal neuron at progressively more depolarizing current injections. (*Lower*) Raw traces (pink) from the same neuron following the addition of Hm1a (10 nM). (Scale bars: 200 ms horizontal; 20 mV vertical.) (*E*) Summary of *i–o* data. Control (black) and Hm1a (pink); $n = 6$. (*F*) No significant change in AP amplitude, rise, width, or threshold was detected at rheobase with only a small depolarizing shift in resting membrane potential ($P < 0.04$, $n = 6$, paired *t* test) in mutant CA1 pyramidal neurons shown without (black bars) and with (pink bars) Hm1a.

NEUROSCIENCE

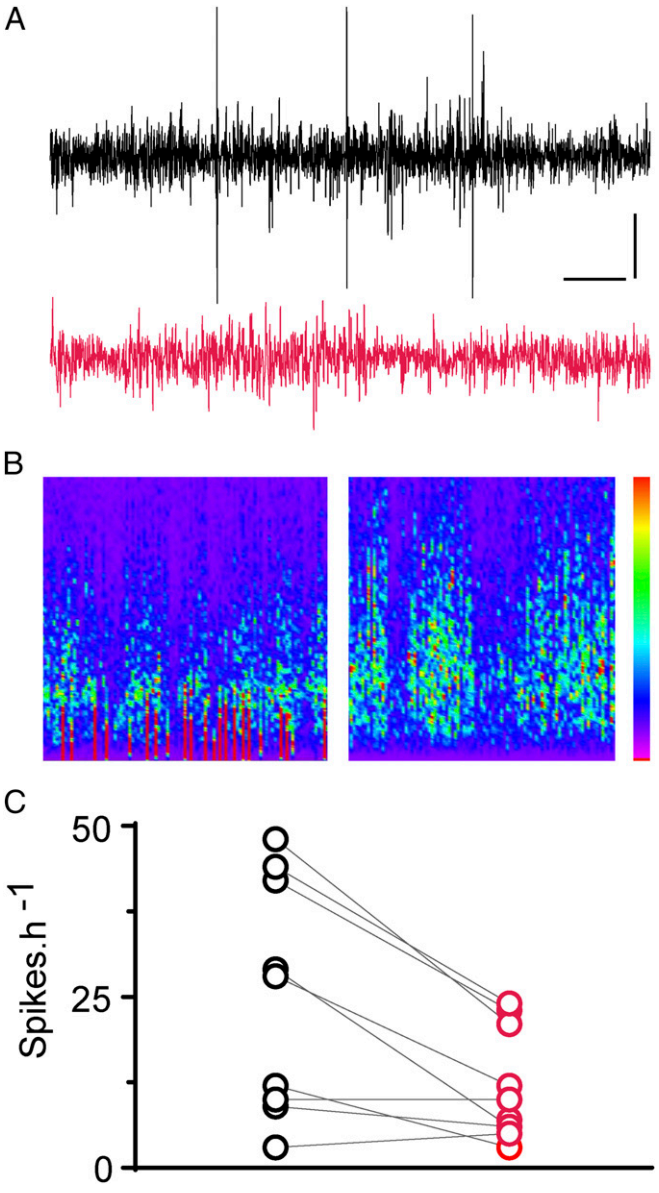

Fig. 6. Hm1a significantly reduced epileptiform discharges in Dravet syndrome mice. Example of an interictal ECoG recording pre- and post-Hm1a infusion from a P20 Dravet syndrome mouse. (*A*, *Upper*) In the raw trace before Hm1a delivery (black), a 10-min ECoG recording displays spontaneous high-amplitude (>400 μV) interictal spikes. (*Lower*) The raw trace from same animal after ICV infusion of Hm1a (pink) showing loss of high-amplitude spikes. (Scale bars: 1 min horizontal; 200 μV vertical.) (*B*) Spectral analysis for a 30-min epoch visualized as a color power spectrum [frequency in Hz (*y* axis) versus time (*x* axis)] illustrates peak activity in 0.5–2 Hz before Hm1a delivery (*Left*) versus a marked reduction in activity for the 30-min epoch recorded post-Hm1a infusion (*Right*). The color key ranges from −20 to 200 μV^2. (*C*) Mean spike count per hour before (black circles) and after (pink circles) Hm1a infusion in Dravet syndrome mice. Hm1a significantly reduced mean spike frequency from 27.6/h (95% CI 14.7–40.5/h) before Hm1a infusion to 11.7/h (95% CI 5.98–17.4/h) after Hm1a infusion; $P = 0.006$, $n = 9$; paired *t* test).

Interneurons are key regulators of cortical excitability, and their dysfunction is believed to underlie pathology in Dravet syndrome (9, 26). Hm1a was able to rescue AP collapse in fast-spiking Pv^+ inhibitory interneurons from Dravet syndrome mice, ostensibly through its ability to enhance $Na_V1.1$ function. The peptide had no effect on the firing properties of excitatory pyramidal neurons in Dravet syndrome mice. This strongly implies that Hm1a specifically targets the emerging cellular deficit in Dravet syndrome mice. This may also explain the remarkable efficacy of Hm1a in reducing both seizure susceptibility and mortality without apparent adverse effects.

Clinical development of peptide CNS therapeutics in general is difficult. One of the major challenges is that peptides such as Hm1a are not blood–brain barrier permeant; delivery therefore needs to occur via injection into the intrathecal or intracerebroventricular spaces. A number of parameters, including the dynamics of fluid flow from the CSF to the interstitial fluid and half-life, will be critical in determining the final distribution of a peptide within the brain. Hm1a will likely need to be delivered using microinfusion pumps to overcome brain-accessibility problems. Microinfusion of peptides has already been used clinically for intrathecal delivery of ziconotide, a synthetic equivalent of a naturally occurring conopeptide, which is used as an effective, Food and Drug Administration-approved treatment for severe chronic pain (29).

In humans, neonatal/infantile seizure onset in Dravet syndrome often marks disease progression and subsequent comorbidities, including cognitive and behavioral deficits (30). Additional studies will determine if Hm1a therapy can prevent such comorbid states. Furthermore, the molecular and cellular selectivity of Hm1a suggest that it might have a broader application beyond Dravet syndrome and other *SCN1A*-associated epilepsies (31), including intractable temporal lobe epilepsy for which partial loss of Pv^+ interneurons appears to be a pathological hallmark (32). $Na_V1.1$ agonists such as Hm1a might also be useful for the treatment of schizophrenia, in which there appears to be both loss and reduced connectivity of Pv^+ interneurons (33), and Alzheimer's disease in which reduced levels of $Na_V1.1$ in Pv^+ interneurons have been linked to network hyperactivity and cognitive dysfunction (34).

Our data indicate that selective activation of $Na_V1.1$ restores normal network excitability in a genetic model of Dravet syndrome. This precision medicine approach has the potential both to control seizures and to ameliorate Dravet syndrome comorbidities, and it should be applicable to other genetic epilepsies.

Materials and Methods

Tissue Cell Culture and Stable Transfection. HEK293T cells stably transfected with h*SCN1A*, h*SCN2A*, h*SCN3A*, h*SCN5A*, h*SCN9A*, and h*SCN10A* were maintained in DMEM Nutrient Mixture F-12 (Invitrogen) supplemented with 10% (vol/vol) FBS (Invitrogen), 0.9% penicillin/streptomycin (P/S) solution, and 100 μg/mL hygromycin or 100 μg/mL neomycin. CHO cells stably transfected with h*SCN4A* and h*SCN8A* were maintained in Ham's F-12 Nutrient Mixture (Invitrogen) supplemented with 10% (vol/vol) FBS, 0.9% P/S solution, and 100 μg/mL hygromycin. Cells were grown to ∼70% confluency in T25 flasks (BD Biosciences).

Planar Patch-Clamp Electrophysiology. Patch-clamp recordings were made using a Patchliner (Nanion Technologies) in the whole-cell configuration. Before recordings, cells were detached from culture flasks with Accutase Cell Detachment Solution (Innovative Cell Technologies Inc.) and resuspended at a density of 1×10^6 to 5×10^7 cells/mL in 50% serum-free medium and 50% external recording solution (vol/vol). The external recording solution comprised (in mM) 140 NaCl, 4 KCl, 1 $MgCl_2$, 2 $CaCl_2$, 5 D-glucose, 10 Hepes (pH 7.4) with NaOH, 298 mOsm. The internal recording solution comprised (in mM) 50 CsCl, 60 CsF, 10 NaCl, 20 EGTA, 10 Hepes (pH 7.2) with CsOH, 285 mOsm. High-fidelity seals were established through brief exposure to a high-calcium–containing solution comprising (in mM) 80 NaCl, 35 $CaCl_2$, 10 $MgCl_2$, 3 KCl, 10 Hepes (pH 7.4) with HCl, 298 mOsm. Solutions were filtered using a 0.2-μm membrane filter (Minisart; Sartorius Stedim Biotech). Cells were kept in suspension by automatic pipetting. Hm1a was dissolved in H_2O with 0.1% fatty acid-free BSA (fafBSA) (Sigma-Aldrich). Medium single-hole planar NPC-16 chips with an average resistance of ∼2.5 MΩ were used. Chip and whole-cell capacitance were fully compensated, and 50% series resistance compensation was applied. Recordings were acquired at 50 kHz with the low-pass filter set to 10 kHz in PATCHMASTER (HEKA Instruments) and performed at 27 °C. When data needed further filtering for the analysis of sustained current, recordings were additionally filtered

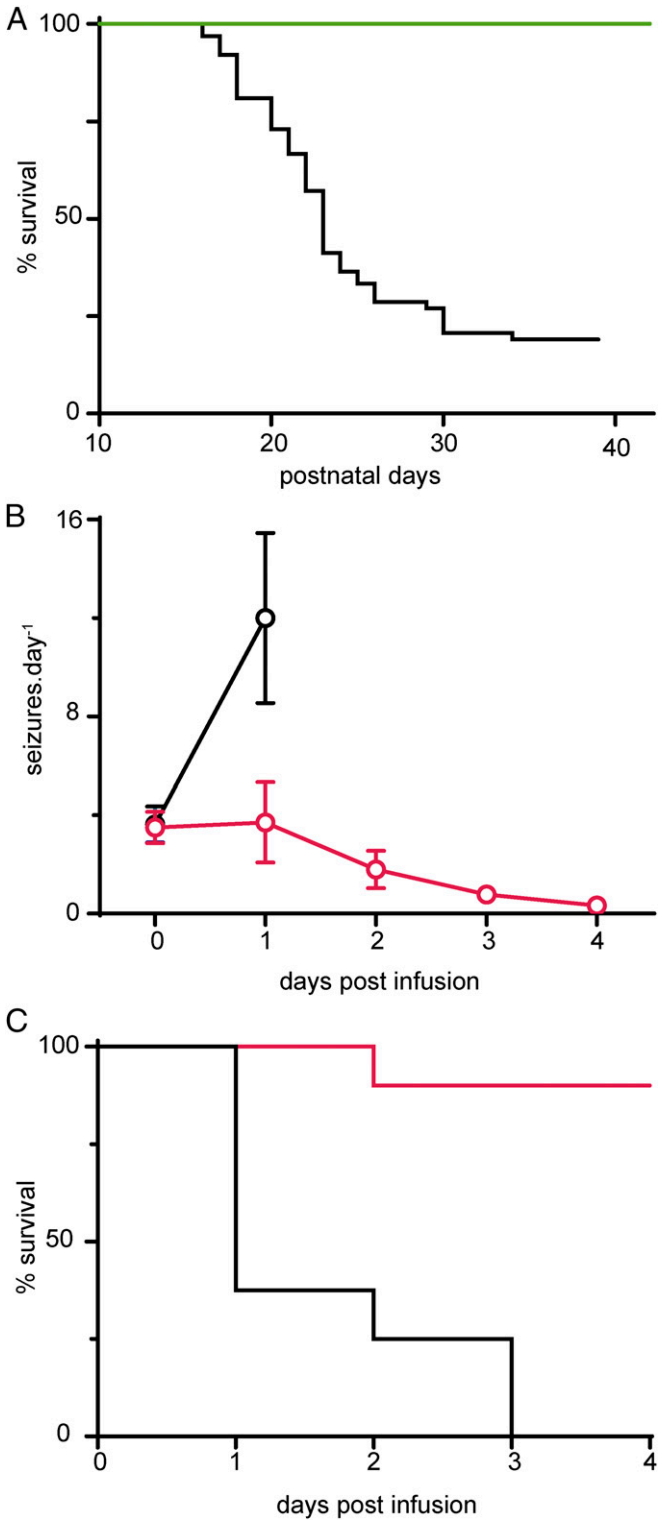

Fig. 7. Hm1a significantly reduces seizure number and postictal mortality in Dravet syndrome mice. (*A*) Survival curves for standard-housed heterozygous Dravet syndrome mice (black trace; $n = 45$) compared with WT littermates (green trace; $n = 20$) revealed significantly increased mortality in Dravet syndrome mice ($P < 0.0001$; Mantel–Cox test). The highest mortality of Dravet syndrome mice occurred between P18 and P26; thus long-term Hm1a efficacy was assessed during the critical epileptogenic period. (*B*) Mean seizure count for Dravet syndrome mice randomly assigned to either vehicle treatment (control, black circles) [3.63 (95% CI 1.90–5.35); $n = 8$] or Hm1a treatment (pink circles) [3.50 (95% CI 2.06–4.94); $P = 0.96$; $n = 10$] was not significantly different before ICV infusion of Hm1a (day 0). At day 1 post-infusion, the mean seizure count for vehicle-treated control mice [12.00 (95% CI 3.82–20.18)] was significantly higher than for Hm1a-treated mice [3.70 (95% CI 0.005–7.40); $P = 0.003$]. The majority of Dravet syndrome mice were seizure free after 3 d of continuous Hm1a infusion. (*C*) Survival curves for Dravet syndrome mice treated with vehicle (black trace) or Hm1a (pink trace). Ninety percent of Hm1a-treated mice were alive at day 3, whereas no vehicle-treated mice survived to day 3. Data are mean ± SEM.

at 500 Hz offline using a Gaussian filter algorithm. Offline analysis was performed using Microsoft Excel, MATLAB R2015a (MathWorks), Igor Pro-6.37 (WaveMetrics Inc.), and GraphPad Prism 7 (Molecular Devices). Biophysical analysis was performed using tailored MATLAB scripts. Currents were normalized after leak subtraction. The area under the curve (AUC) was used to measure the efficacy and sensitivity of Hm1a for $Na_V1.1$ and $Na_V1.3$. Efficacy was calculated as a mean percentage change (%) using the area of the negative peaks under the raw current traces with the baseline set at zero. Efficacy describes the magnitude of the change in total charge, a combination of delayed inactivation and increased current amplitude. Sensitivity was calculated from the mean normalized AUC as a change in response versus concentration, essentially producing a concentration–response curve.

Pulse Protocols. Electrophysiological protocols were as previously described (35). Briefly, the voltage dependence of activation was studied by measuring normalized peak currents during 100-ms depolarizations from −120 mV to +30 mV in 5-mV increments. The resulting current–voltage curve was fit to the equation $I = (1 + \exp[-x(V - V_{0.5})]/g(V - V_r))$, where I is the current amplitude, z is the apparent gating charge, V is the test potential, $V_{0.5}$ is the half-maximal voltage, g is a factor related to the maximum number of open channels, and V_r is the reversal potential. Conductance (G) was determined using $G = I/(V - V_r)$. Calculated conductance values were then fit with the Boltzmann equation $G = 1/(1 + \exp[(V - V_{0.5})/a])$, where a is the slope of the half-maximum, V is the potential of the given pulse, and $V_{0.5}$ is the potential for the half-maximal activation. To study steady-state fast inactivation, cells were held at conditioning prepulse potentials ranging from −120 mV to +30 mV in 5-mV increments from a holding potential of −120 mV and a test pulse at 5 mV for 20 ms. Peak currents (I) during the subsequent test pulses were normalized to the peak current during the first test pulse (I_{max}) and were plotted against the potential of the conditioning pulse and fitted with the Boltzmann equation $I/I_{max} = 1/(1 + \exp[(V - V_{0.5}]/a)$. Inactivation time constants were determined using an IGOR script that identified the peak current of each trace. The data were fit with a double exponential function $I/Imax = I_0 + A_1{*}\exp(-t-t0/\tau1) + A_2{*}\exp(-t-t0/\tau2)$, where I_0 is the non-inactivating component, $Imax$ is the peak current, t is time, and A_1 and A_2 are the components for the time constants $\tau1$ and $\tau2$, respectively. Time constants were plotted against voltage, and the data were fitted with a decaying exponential equation $Y = span \times \exp(-Kx) + plateau$, where $span$ is the starting point of the curve, K is the decay factor, $plateau$ is the value to which the curve decays, and x is time. Recovery from fast inactivation was studied by prepulsing the cells to 0 mV from a holding potential of −120 mV for 30 ms to fully inactivate channels. The voltage was then stepped back to the holding potential for variable interpulse intervals (ipi) from 0 to 39 ms in 3-ms increments. To test channel availability, the voltage was stepped to 0 mV for 30 ms. Peak current (I) was plotted as fractional recovery against the recovery period by normalizing to the maximum current (I_{max}) during the conditioning potentials. Recovery currents were plotted against ipi, and data were fitted with the equation $I/I_{max} = 1 - \exp/(rc + x)$, where I_{max} is maximum current, rc is the recovery rate constant, and x is time.

To examine the effects of Hm1a on $hNa_V1.1$–1.8, cells were held at −120 mV, and 20- or 100-ms test depolarizations to 0 mV were applied every 2 s for 60 s in the presence of vehicle control (0.1% fafBSA). The cells were then exposed to 1, 5, or 50 nM Hm1a sequentially for 2 min. Currents for individual cells were averaged over 30-s periods directly before the application of Hm1a and following a 2-min exposure to 1, 5, or 50 nM Hm1a. To determine EC_{50} values for the effects of Hm1a on $hNa_V1.1$ and $hNa_V1.3$, cells were held at −80 mV, stepped to −120 mV for 200 ms followed by 50-ms test depolarization to 0 mV every 2 s for 60 s in the presence of vehicle control (0.1% fafBSA). The cells were then exposed to Hm1a (0.3–3000 nM) sequentially for 2 min.

Hm1a Structure. Hm1a (300 μL of a 1-mM solution in 95% H_2O/5% D_2O, pH 4) was placed in a susceptibility-matched Shigemi microcell, and NMR spectra were acquired at 900 MHz on a Bruker AVANCE spectrometer

NEUROSCIENCE

equipped with a cryogenic probe. 2D ^{1}H-^{1}H total correlation spectroscopy (TOCSY) [mixing time (τ) = 80 ms], ^{1}H-^{1}H NOESY (τ = 250 ms), ^{1}H-^{13}C heteronuclear single quantum coherence (HSQC), and ^{1}H-^{15}N HSQC NMR were acquired with WATERGATE water suppression used in homonuclear NMR experiments. Sequence-specific resonance assignments were made using CcpNmr (36); chemical shifts have been deposited in the Biological Magnetic Resonance Data Bank (accession no. 25775). Backbone dihedral-angle restraints for structure calculations were obtained from TALOS+ chemical shift analysis (37). NOESY cross-peaks were manually picked and integrated; then CYANA 3.0 (38) was used to automatically assign NOESY peaks and calculate a structural ensemble. Using a tolerance of 0.02 ppm and 0.025 ppm in the direct and indirect dimensions, respectively, CYANA assigned 94.3% of 1,314 NOESY cross-peaks. CYANA was used to calculate 300 structures from random starting conformations; then the 30 best-ranked structures were evaluated by MolProbity (39) to generate an ensemble consisting of the 20 conformers with highest stereochemical quality. Atomic coordinates are available from the Protein Data Bank (ID code 2N6O).

Hm1a Stability. CSF was obtained from patients undergoing lumbar puncture at St. Vincent's Hospital, Sydney (Ethics Approval SVH15/024) and informed consent was obtained from all participants. Hm1a was added to human CSF (final concentration 0.5 μM); then the sample was incubated at 37 °C for up to 3 d (Human Research Ethics Approval UQ 20160008176). Samples were collected at various time points; then the reaction was quenched and proteins were precipitated by the addition of 5% trifluoroacetic acid. Samples were centrifuged at 25,000 × *g* for 10 min at 4 °C; then 20 μL of the supernatant was transferred to a new tube containing 5% formic acid (FA), and the sample was centrifuged again at 25,000 × *g* for 20 min at 4 °C. The supernatant (10 μL) was then processed [150 mm × 2.1 mm; flow rate 0.2 mL/min; gradient of 2–40% solvent B (90% acetonitrile, 0.1% FA) in solvent A (0.1% FA) over 14 min] coupled to a TripleTOF 5600 mass spectrometer (AB SCIEX) with a cycle time of 0.2751 s. Peak areas were measured for triple-, quadruple-, and quintuple-charge states and were analyzed using PeakView and MultiQuant (Sciex) software. hANP (1 μM; GenScript) and ziconotide (ω-conotoxin MVIIA, 1 μM; Alomone Labs) served as controls.

Mice. Mice were housed in a temperature-controlled environment maintained at 23 °C with a 12-h light/dark cycle. *Scn1a* (R1407X) Dravet syndrome mice were maintained on the 129S1/SvImJ background and were crossed to the C57BL/6J (N2) background for experiments. At P7, mice were genotyped using the PCR protocol described previously (9). Mice for electrophysiology experiments were used at P14–P16. Mice aged P18–P26 were used for in vivo animal experiments.

Brain Slice Electrophysiology. Heterozygote Dravet syndrome mice and WT littermates (P14–P16) were anesthetized using isoflurane and were killed by decapitation. Brain slices (300 μm thick) were cut using a vibratome in the sagittal plane. Slices were kept at room temperature until recording. The slices were transferred to a recording chamber constantly perfused at 34 °C with artificial CSF solution consisting of (in mM): 125 NaCl, 2.5 KCl, 25 $NaHCO_3$, 1.25 NaH_2PO_4, 1 $MgCl_2$, 2 $CaCl_2$, and 10 glucose, aerated with 95% O_2 and 5% CO_2 to a final pH of 7.4. Hm1a (10 nM) was dissolved in H_2O with 0.1% fafBSA (Sigma-Aldrich). Whole-cell patch-clamp recordings were made using a MultiClamp 700A amplifier and pClamp acquisition software (Molecular Devices) from neurons visually identified using infrared differential interference contrast imaging (BX51; Olympus). Electrodes were pulled using a Sutter P-2000 puller (Sutter Instruments) from borosilicate micropipettes (World Precision Instruments) with an initial resistance of ∼2–3 MΩ and filled with intracellular solution consisting of (in mM): 125 KGlu, 4 KCl, 2 $MgCl_2$, 10 Hepes, 10 EGTA, 4 ATP-Mg, 0.3 GTP-Na, 8 biocytin hydrochloride, adjusted to a final pH of 7.3 with KOH. D-Mannitol was used to adjust osmolarity to 300 mOsm. Bridge balance and capacitance compensation was applied to all recordings. Voltage recordings were filtered at 30 kHz and sampled at 100 kHz. A holding current was injected into neurons if required, setting their holding potential to approximately −75 mV. An *i–o* relationship was established by injecting an 800-ms square pulse of progressively depolarizing currents. An automated AP detection algorithm in AxoGraph was used to detect APs with visual confirmation. The integrated number of APs between injection current bins of the *i–o* relationships was calculated (AxoGraph X) to allow comparison between control and Hm1a treatment. The AP threshold voltage was defined as the voltage at which the gradient reached 10 $mV{\cdot}ms^{-1}$. For AP waveform analysis, amplitude was measured from threshold to peak, rise time was defined as the time between 10–90% of the AP amplitude, and AP width measurements were made at 50% of the peak amplitude. APs measured at collapse were selected for each individual cell at the first current injection at which AP collapse was robust. APs at the same current injection were analyzed in the presence of Hm1a. Membrane input resistance was estimated in current clamp by measuring the last 200 ms of the voltage trace generated by a −10 pA current injection.

ECoG and ICV Guide Cannula Surgery. Heterozygote *Scn1a* (R1407X) Dravet syndrome mice and WT littermates underwent ECoG and ICV guide cannula implantation surgery at P18. ECoG surgery was performed as previously described (40); in addition, a guide cannula was implanted and positioned in the right ventricle using a Kopf stereotaxic frame with the following coordinates: caudal −0.2 mm and lateral 1.0 mm from bregma; 2.0 mm from the skull. At least 24-h recovery followed surgery before commencing ECoG recording and simultaneous infusion of peptide or vehicle alone delivered via ICV. A total volume of 5 μL of peptide (0.5 μM), suspended in vehicle containing 0.1% fafBSA and sterile saline was infused; control animals received 5 μL of vehicle only. Peptide or vehicle only was infused (0.1–0.2 μL/min) via an internal cannula connected to a Hamilton syringe and driver (Harvard PHD 2000). Placement of the ICV cannula and the injection site was validated using blue dye delivered via the right ventricle and post hoc analysis of experimental animals.

For ECoG experiments, recordings were made in animals at least 1 h before Hm1a ICV delivery and then an additional 2–3 h after Hm1a infusion using PowerLab 16/30 (ADInstruments); signals were bandpass filtered at 0.1–200 Hz and sampled at 1 kHz. A criterion for measurement of interictal spikes was an amplitude at least two times greater than the SD of the background ECoG signal. Examples of the interictal and spontaneous ictus events are provided in *SI Appendix*, Fig. S5. Power spectrum analyses for 30-min epoch and frequency components were calculated by conventional fast Fourier transformation and were analyzed using Sirenia Seizure Pro (1.6.6; Pinnacle Technology).

To examine the ability of Hm1a to modulate seizures in the long term, animals were video-monitored for seizure events at least 24 h after ICV guide cannula surgery. Animals with at least two seizure events were assigned to either the Hm1a-treated or vehicle-treated control group; solutions [either vehicle (saline/fafBSA) or Hm1a (0.5 μM in vehicle)] were delivered continuously for up to 5 d via ICV with a flow rate 0.2 μL/min using a Hamilton syringe and driver. Seizure frequency and survival were measured using continuous video recordings of ICV-tethered animals from P19. Video recording was done using a Vivotek video server (VS8102) connected to an infrared day and night digital color camera (EVO2; Pacific Communications). Two independent observers conducted long-term infusion experiments and analyzed digital video images offline. During experiments mice were housed individually with a 12-h light/dark cycle and ad libitum access to water and food.

Statistical Analyses. All statistical analyses were performed using GraphPad Prism 7 (Molecular Devices) software, with a P value <0.05 considered statistically significant. Data values are expressed as mean ± SEM. Comparisons between datasets were made using a paired or unpaired Student's *t* test; survival curves were created using the Kaplan–Meier method and evaluated using a Mantel–Cox test. One-way ANOVA with Bonferroni correction was applied to take into account multiple comparisons in Figs. 1 and 2.

Study Approval. All animal experiments were approved by the Animal Ethics Committee, Florey Institute of Neuroscience and Mental Health (approval nos. 13-097 and 14-046) and were conducted in accordance with the guidelines of the National Health and Medical Research Council Code of Practice for the Care and Use of Animals for Experimental Purposes in Australia.

ACKNOWLEDGMENTS. We thank Prof. Kazuhiro Yamakawa (RIKEN Brain Science Institute) for donating Dravet syndrome mice and Prof. Gilles Guillemin (St Vincent's Centre for Applied Medical Research) for human CSF. This work was supported by Citizen's United for Research in Epilepsy Pediatrics Award 353711, Australian National Health and Medical Research Council Program Grant 10915693 (to S.P. and C.A.R.), Principal Research Fellowships (to S.P. and G.F.K.), an Australian Research Council Discovery Early Career Researcher Award Fellowship (to E.A.B.U.), a Dowd Foundation Research Fellowship (to C.A.R.), and by the GINOP-2.3.2-15-2016-00044 Project cofinanced by the European Union and the European Regional Development Fund (G.P.). The Florey Institute of Neuroscience and Mental Health is supported by infrastructure funds from the Department of Health, State Government of Victoria.

1. Dravet C (2011) The core Dravet syndrome phenotype. *Epilepsia* 52:3–9.
2. Scheffer IE (2012) Diagnosis and long-term course of Dravet syndrome. *Eur J Paediatr Neurol* 16(Suppl 1):S5–S8.
3. Higurashi N, Uchida T, Hirose S, Okano H (2013) Current trends in Dravet syndrome research. *J Neurol Neurophysiol* 4:152.
4. Kalume F (2013) Sudden unexpected death in Dravet syndrome: Respiratory and other physiological dysfunctions. *Respir Physiol Neurobiol* 189:324–328.
5. Brigo F, Igwe SC, Bragazzi NL (2017) Antiepileptic drugs for the treatment of infants with severe myoclonic epilepsy. *Cochrane Database Syst Rev* 5:CD010483.
6. Shmuely S, Sisodiya SM, Gunning WB, Sander JW, Thijs RD (2016) Mortality in Dravet syndrome: A review. *Epilepsy Behav* 64:69–74.
7. De Jonghe P (2011) Molecular genetics of Dravet syndrome. *Dev Med Child Neurol* 53: 7–10.
8. Gataullina S, Dulac O (2017) From genotype to phenotype in Dravet disease. *Seizure* 44:58–64.
9. Ogiwara I, et al. (2007) $Na_V1.1$ localizes to axons of parvalbumin-positive inhibitory interneurons: A circuit basis for epileptic seizures in mice carrying an *Scn1a* gene mutation. *J Neurosci* 27:5903–5914.
10. Catterall WA (2014) Sodium channels, inherited epilepsy, and antiepileptic drugs. *Annu Rev Pharmacol Toxicol* 54:317–338.
11. Cheah CS, et al. (2012) Specific deletion of $Na_V1.1$ sodium channels in inhibitory interneurons causes seizures and premature death in a mouse model of Dravet syndrome. *Proc Natl Acad Sci USA* 109:14646–14651.
12. Han S, et al. (2012) Autistic-like behaviour in *Scn1a*$^{+/-}$ mice and rescue by enhanced GABA-mediated neurotransmission. *Nature* 489:385–390.
13. Ogiwara I, et al. (2013) Nav1.1 haploinsufficiency in excitatory neurons ameliorates seizure-associated sudden death in a mouse model of Dravet syndrome. *Hum Mol Genet* 22:4784–4804.
14. Wallace A, Wirrell E, Kenney-Jung DL (2016) Pharmacotherapy for Dravet syndrome. *Paediatr Drugs* 18:197–208.
15. Plosker GL (2012) Stiripentol : In severe myoclonic epilepsy of infancy (Dravet syndrome). *CNS Drugs* 26:993–1001.
16. Osteen JD, et al. (2016) Selective spider toxins reveal a role for the $Na_V1.1$ channel in mechanical pain. *Nature* 534:494–499.
17. Osteen JD, Sampson K, Iyer V, Julius D, Bosmans F (2017) Pharmacology of the $Na_V1.1$ domain IV voltage sensor reveals coupling between inactivation gating processes. *Proc Natl Acad Sci USA* 114:6836–6841.
18. Zhang MM, et al. (2013) Co-expression of $Na_V\beta$ subunits alters the kinetics of inhibition of voltage-gated sodium channels by pore-blocking μ-conotoxins. *Br J Pharmacol* 168:1597–1610.
19. Bosmans F, Milescu M, Swartz KJ (2011) Palmitoylation influences the function and pharmacology of sodium channels. *Proc Natl Acad Sci USA* 108:20213–20218.
20. Escoubas P, Diochot S, Célérier ML, Nakajima T, Lazdunski M (2002) Novel tarantula toxins for subtypes of voltage-dependent potassium channels in the Kv2 and Kv4 subfamilies. *Mol Pharmacol* 62:48–57.
21. Kwan AH, Mobli M, Gooley PR, King GF, Mackay JP (2011) Macromolecular NMR spectroscopy for the non-spectroscopist. *FEBS J* 278:687–703.
22. Pallaghy PK, Nielsen KJ, Craik DJ, Norton RS (1994) A common structural motif incorporating a cystine knot and a triple-stranded β-sheet in toxic and inhibitory polypeptides. *Protein Sci* 3:1833–1839.
23. Kintzing JR, Cochran JR (2016) Engineered knottin peptides as diagnostics, therapeutics, and drug delivery vehicles. *Curr Opin Chem Biol* 34:143–150.
24. Sanford M (2013) Intrathecal ziconotide: A review of its use in patients with chronic pain refractory to other systemic or intrathecal analgesics. *CNS Drugs* 27:989–1002.
25. Cao D, et al. (2012) Efficacy of stiripentol in hyperthermia-induced seizures in a mouse model of Dravet syndrome. *Epilepsia* 53:1140–1145.
26. Yu FH, et al. (2006) Reduced sodium current in GABAergic interneurons in a mouse model of severe myoclonic epilepsy in infancy. *Nat Neurosci* 9:1142–1149.
27. Cheah CS, et al. (2013) Correlations in timing of sodium channel expression, epilepsy, and sudden death in Dravet syndrome. *Channels (Austin)* 7:468–472.
28. Gazina EV, et al. (2010) Differential expression of exon 5 splice variants of sodium channel α subunit mRNAs in the developing mouse brain. *Neuroscience* 166:195–200.
29. Pope JE, Deer TR (2015) Intrathecal pharmacology update: Novel dosing strategy for intrathecal monotherapy ziconotide on efficacy and sustainability. *Neuromodulation* 18:414–420.
30. Ito S, et al. (2013) Mouse with $Na_V1.1$ haploinsufficiency, a model for Dravet syndrome, exhibits lowered sociability and learning impairment. *Neurobiol Dis* 49:29–40.
31. Parihar R, Ganesh S (2013) The SCN1A gene variants and epileptic encephalopathies. *J Hum Genet* 58:573–580.
32. Andrioli A, Alonso-Nanclares L, Arellano JI, DeFelipe J (2007) Quantitative analysis of parvalbumin-immunoreactive cells in the human epileptic hippocampus. *Neuroscience* 149:131–143.
33. Jensen HS, Grunnet M, Bastlund JF (2014) Therapeutic potential of $Na_V1.1$ activators. *Trends Pharmacol Sci* 35:113–118.
34. Verret L, et al. (2012) Inhibitory interneuron deficit links altered network activity and cognitive dysfunction in Alzheimer model. *Cell* 149:708–721.
35. Oliva MK, et al. (2014) Physiological and genetic analysis of multiple sodium channel variants in a model of genetic absence epilepsy. *Neurobiol Dis* 67:180–190.
36. Vranken WF, et al. (2005) The CCPN data model for NMR spectroscopy: Development of a software pipeline. *Proteins* 59:687–696.
37. Shen Y, Delaglio F, Cornilescu G, Bax A (2009) TALOS+: A hybrid method for predicting protein backbone torsion angles from NMR chemical shifts. *J Biomol NMR* 44: 213–223.
38. Güntert P (2004) Automated NMR structure calculation with CYANA. *Methods Mol Biol* 278:353–378.
39. Davis IW, et al. (2007) MolProbity: All-atom contacts and structure validation for proteins and nucleic acids. *Nucleic Acids Res* 35:W375–W383.
40. Tan HO, et al. (2007) Reduced cortical inhibition in a mouse model of familial childhood absence epilepsy. *Proc Natl Acad Sci USA* 104:17536–17541.